Journal of Power Sources 185 (2008) 1392–1397

Contents lists available at ScienceDirect

Journal of Power Sources

journal homepage: www.elsevier.com/locate/jpowsour

Lithium anode for lithium-air secondary batteries

Nobuyuki Imanishi*, Satoshi Hasegawa, Tao Zhang, Atushi Hirano, Yasuo Takeda, Osamu Yamamoto

Department of Chemistry, Faculty of Engineering, Mie University, 1577 Kurimamachiacho, Tsu, Mie 514-8507, Japan

ARTICLE INFO

Article history:
Received 24 April 2008
Received in revised form 28 July 2008
Accepted 29 July 2008
Available online 6 August 2008

Keywords:
Lithium ion conductor
Solid electrolyte
LiPON
Lithium anode

ABSTRACT

The lithium ion conducting solid lithium phosphorous nitride (LiPON) has been sputtered on the water-stable NASICON-type lithium ion conducting solid electrolyte $Li_{1+x+y}Al_xTi_{2-x}P_{3-y}Si_yO_{12}$ (LATP). The stability and the interface resistance of the Li–Al/LiPON/LATP/LiPON/Li–Al cell have been examined. It is shown that the LiPON film protects LATP from reacting with the Li–Al alloy. The impedance of the Li–Al/LiPON/LATP/LiPON/Li–Al cell has been measured in the temperature range 25–80 °C. The total cell resistance is about 8600 Ω cm^2 at room temperature and 360 Ω cm^2 at 80 °C. The analysis of the impedance profiles suggests that the Li–Al/LiPON interface resistance is dominant at lower temperatures. The LATP plate immersed in water for 1 month shows only a slight degradation in the conductivity.

1. Introduction

The lithium-air battery possesses the highest theoretical gravimetric energy density among the possible electrochemical power sources. The theoretical specific energy of Li-air excluding oxygen is 11.5 kWh kg^{-1}, the value of which is comparable with that of gasoline/air device [1,2]. This high energy density battery has the potential to be the power source for the advanced electric vehicles. The lithium-air secondary battery with the gel-type lithium conducting polymer electrolyte was first reported in 1996 by Abraham and Jiang [1]. This prototype cell showed an open circuit voltage of about 3 V and oxygen electrode capacity of 1600 mAh g^{-1} of carbon. The specific energy density of this cell from the weight of the electrode and the electrolyte was estimated to be 250–350 Wh kg^{-1}. Higher discharge capacity of 2120 mAh g^{-1} of carbon was observed on Super carbon black with liquid organic electrolyte using λ-MnO_2 as the catalyst [3]. More recently, Kuboki et al. [4] reported that an extremely high capacity of 5360 mAh g^{-1} of carbon was observed in the cell with hydrophobic ionic liquid electrolyte using cobalt phthalocyanine as the catalyst. These high air electrode capacities suggest that we have a possibility to obtain the high energy density lithium-air battery of 700 Wh kg^{-1}, the value of which is a final target of the New Energy and Industrial Technology Development Organization (NEDO) project for the batteries in the next generation electric vehicles. Further, the cyclability of the Li-air battery with the organic liquid electrolyte of $LiPF_6$ in propylene carbonate was reported [5]. The oxygen electrode capacity was decreased with cycling, but the capacity of 600 mAh g^{-1} of carbon was maintained after 50 cycles.

These attractive previous results for the Li-air battery were obtained under the pure oxygen or dry oxygen and nitrogen mixture gas. In the practical applications for electrical vehicles, we should use air containing moisture. The perfect exclusion of water in air on the air electrode is difficult and the electrolyte may be contaminated with water. The stability of lithium anode in the electrolyte containing trace water is the most critical point for a long period operation. Recently, Visco et al. [6,7] proposed a unique lithium anode protected by a water-stable lithium conducting solid electrolyte based on the NASICON-type $Li_3M_2(PO_4)_3$ electrolyte. This electrode had operated with an aqueous electrolyte for a long period, and they reported a high stable discharge performance in the Li/solid electrolyte/NH_4Cl in H_2O/air cell for nearly 2 months [7]. The water-stable solid electrolyte is unstable to reduction by lithium metal, so a conductive interlayer is needed. Lithium nitride (Li_3N) and lithium phosphorous oxynitride (LiPON) are the candidates as the interlayer materials, because they show a high lithium ion conductivity and are stable in contact with lithium metal. In this study, the stability and the interface resistance of the lithium/LiPON/$Li_{1+x+y}Al_xTi_{2-x}P_{3-y}Si_yO_{12}$ (LATP) has been examined in a temperature range of 20–80 °C. And also, the stability of the LATP plate in water was examined.

* Corresponding author. Fax: +81 59 231 9478.
E-mail address: imanishi@chem.mie-u.ac.jp (N. Imanishi).

0378-7753/$ – see front matter © 2008 Elsevier B.V. All rights reserved.
doi:10.1016/j.jpowsour.2008.07.080

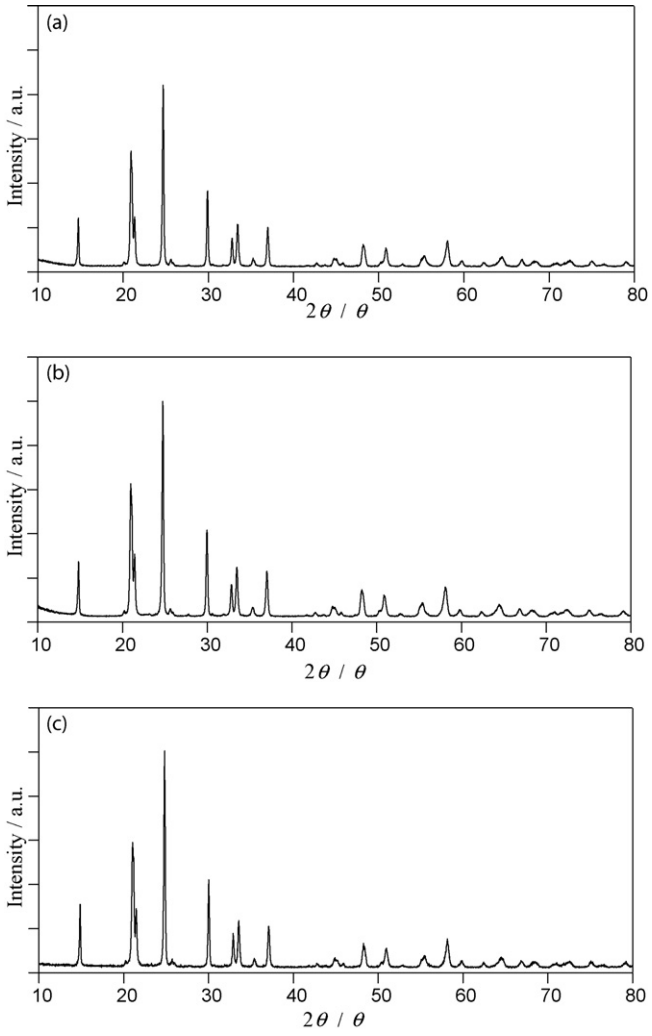

Fig. 1. XRD patterns of the LATP plate (a), the LATP plate with sputtered LATP film (b), and the LATP plate immersed in water for 1 month (c).

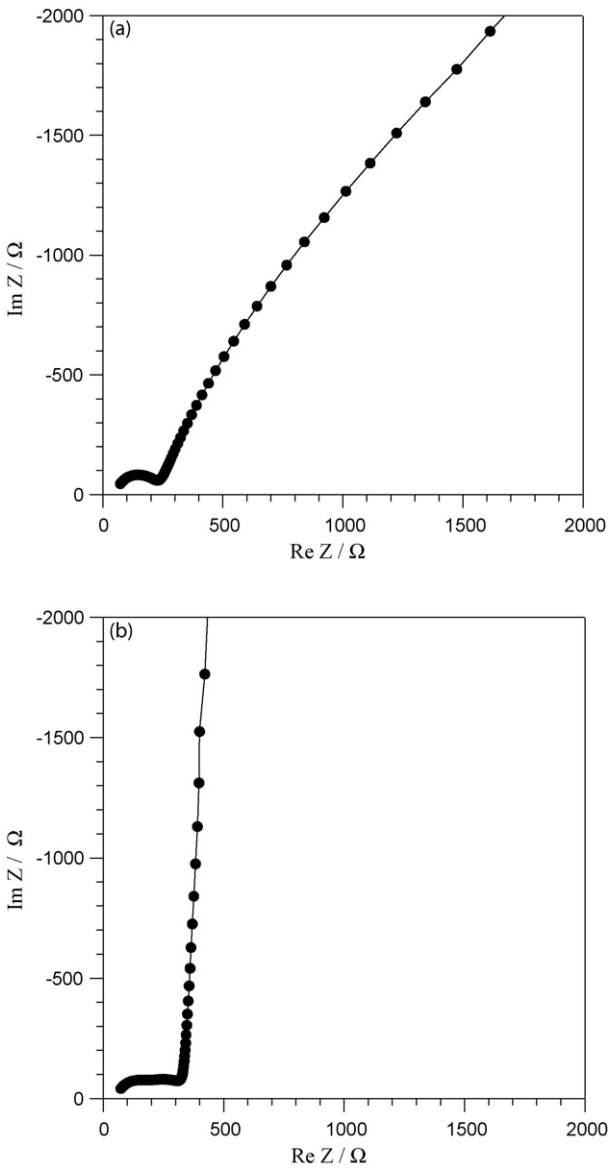

Fig. 2. Impedance spectra at room temperature of the pristine LATP plate (a) and the LATP plate immersed in water for 1 month (b).

2. Experimental

The water-stable NASICON-type lithium ion conducting solid electrolyte, LATP, was supplied by OHARA Inc., Japan. The preparation method of LATP was described in the literature [8,9]. The lithium-stable LiPON electrolyte was deposited on the LATP plate (0.15 mm thick) and the silica glass substrate with a gold electrode (about 0.5 μm thick) by sputtering a Li_3PO_4 target in a nitrogen gas flow. The target was prepared by cold isostatic pressing of a commercial Li_3PO_4 powder (Nacalai Tesque, Inc., Japan). The working pressure was 1.0 Pa and Rf power of 30 W. The distance between the target and the substrate was 7 cm. The deposition rate was about 0.3 μm per hour. To improve the contact between LATP and LiPON, a LATP thin film was sputtered on the surface of the LATP plate using a LATP target, which was prepared by a LATP powder (OHARA Inc.). The gas ratio of Ar/O_2 was 7/3 and pressure was 0.4 Pa. The deposition rate was less than 0.1 μm per hour at a Rf power of 100 W. The LATP plate with the sputtered LATP film was annealed at 900 °C for 8.5 h. The active area for the impedance measurements was 0.36 cm^2.

The impedance of the LATP plate and the LiPON film on silica glass plate were measured with gold electrodes. To make a good contact of the Li metal foil (Honjo Metal Co. Ltd., Japan) with the LiPON film and the LATP plate, an Al thin film was sputtered on the LiPON and the LATP plate surfaces. The symmetrical cell impedances of the Li–Al/LiPON/Li–Al, Li–Al/LATP/Li–Al, Li–Al/LiPON/LATP/LiPON/Li–Al and Au/LiPON/LATP/LiPON/Au cells were measured. The Li–Al/LiPON/Li–Al cell was prepared by sputtering LiPON on the Al sheet (50 μm thick), and then Al sputtered layer was stacked on LiPON. Li sheet was placed on the sputtered layer, and Li metal was deposited on the counter Al sheet by galvanostatic electrolysis. The impedance measurements on the cell were carried out using a Solartron 1260 frequency response analyzer with a Solartron 1287 electrochemical interface in the frequency range of 0.1–1 MHz. The Z-plot software was employed for data analysis and presentation. The ac impedances of the samples were measured in the temperature range of 25–80 °C.

X-ray diffraction (XRD) data were obtained using a Rigaku RINT 2500 X-ray diffractometer with a rotating copper cathode. Scanning electron microscope (SEM) images were measured using Hitachi SEM S-4000.

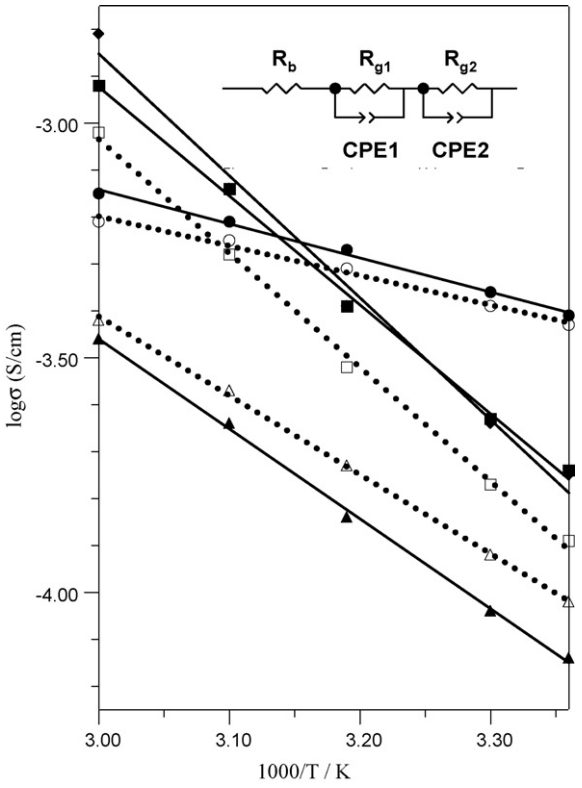

Fig. 3. Temperature dependence of the electrical conductivity of the pristine LATP plate and the LATP plate immersed in water for 1 month. (○) Grain bulk conductivity of LATP, $1/R_b$, (□) grain boundary conductivity of LATP, $1/R_{g1}$, (△) total conductivity of LATP, $1/(R_b + R_{g1})$, (●) grain bulk conductivity of LATP immersed in water, $1/R_b$, (■) grain boundary conductivity of LATP immersed in water, $1/R_{g1}$, (♦) grain boundary conductivity of LATP immersed in water, $1/R_{g2}$, and (▲) total conductivity of LATP immersed in water, $1/(R_b + R_{g1} + R_{g2})$.

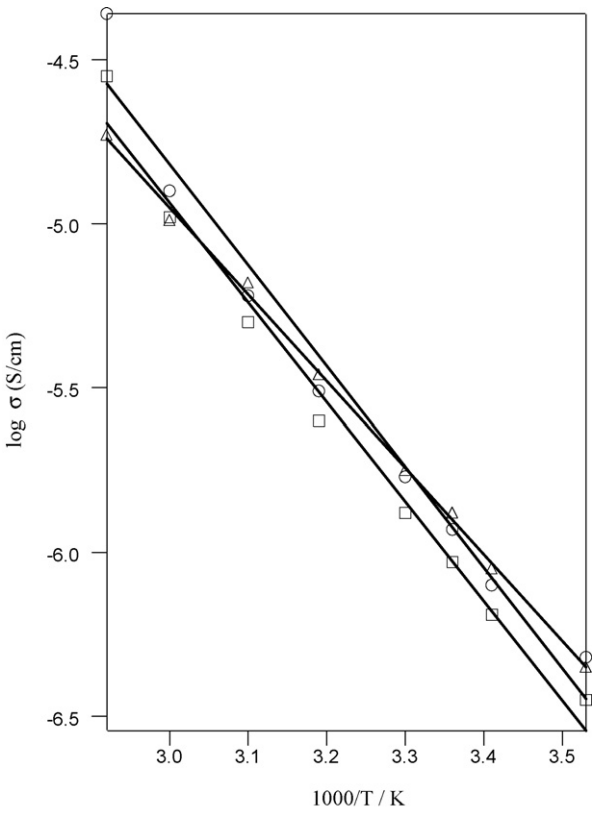

Fig. 4. Temperature dependence of electrical conductivity of the LiPON thin film sputtered on a silica glass plate for various sputtering periods. (○) 3 h, (△) 6 h, and (□) 12 h.

3. Results and discussion

Fig. 1 shows the XRD patterns of the LATP plate supplied from OHARA Inc. and of that sputtered LATP thin film on the surface. The sputtered film was heated at 900 °C for 8.5 h. The thickness of the film was estimated about 50 nm from the AFM image. The XRD patterns of the LATP plate are mainly due to those of the NASICON-type $LiTi_2(PO_4)_3$ phase. The LATP plate with the sputtered LATP film shows the same diffraction patterns. The LATP plate was immersed in distilled water for 1 month at room temperature to assess the stability against water. The XRD patterns of the sample are shown in Fig. 1(c). As shown in these XRD patterns, no significant difference is observed between the pristine and the LATP plates immersed in water for 1 month. The water-stability test of the LATP glass ceramics, primarily consisting of $Li_{1-x}Ti_{2-x}Al_x(PO_4)_3$ $(x - 0.3)$, was also reported very stable in tap water by Thokchom and Kumar [10]. We have confirmed that the LATP plate used in this study is obviously very stable in water in a view point of the XRD study.

Fig. 2 shows the ac impedance spectra of the pristine LATP plate and the LATP plate immersed in water for 1 month at room temperature. The spectrum of the pristine LATP plate reveals one semicircle, which could be attributed to a grain boundary resistance. The intercept of the semicircle on the real axis at a higher frequency represents the resistance of the grain bulk (R_b) and that at lower frequency shows the total resistance of the grain bulk and grain boundary (R_g). The linear Warburg element following the semicircle may be attributed to specimen–electrode interaction [10].

The electrical conductivity of the LATP plate at 25 °C is estimated to be 1×10^{-4} S cm^{-1} for the total and 4.5×10^{-4} S cm^{-1} for the bulk, which is comparable with those previously reported [10–12]. The samples immersed in water for 1 month show a dispersed semicircle and a steeper straight line corresponding to the onset of finite length diffusion. The bulk conductivity is almost same with that of the pristine LATP plate. The dispersed semicircle reflects that the different type of grain boundaries were present by the reaction of LATP with water. The total grain boundary resistance was slightly higher than that of the pristine LATP plate. These results suggest that water react with LATP and a resistive layer was formed at the grain boundary. However, the conductivity degradation by the reaction of LATP with water is not so significant. The temperature dependences of the total conductivity, grain boundary conductivity, and grain bulk conductivity of the pristine LATP plate and the LATP immersed in water for 1 month are shown in Fig. 3. The grain boundary conductivity of the LATP plate immersed in water was estimated using the equivalent circuit model shown in Fig. 3. The activation energy for bulk conductivity of the pristine LATP plate was 16 kJ mol^{-1} and that for grain boundary (R_{g1}) was 49 kJ mol^{-1}, and the second component (R_{g2}) of the grain boundary observed in the LATP plate immersed in water showed the same activation energy for conduction.

LiPON films were deposited on silica glass plate with an Au film as the electrode by Rf magnetron sputtering for 3–12 h. The obtained films showed only amorphous XRD patterns. Fig. 4 shows the temperature dependence of the electrical conductivity of the sputtered LiPON films with different thickness, where the thickness of the LiPON film was estimated from the weight gain and the SEM image. They were 0.9, 1.1, and 3.1 μm for 3, 6, 12 h of sputtering period, respectively. The electrical conductivity at 25 °C is

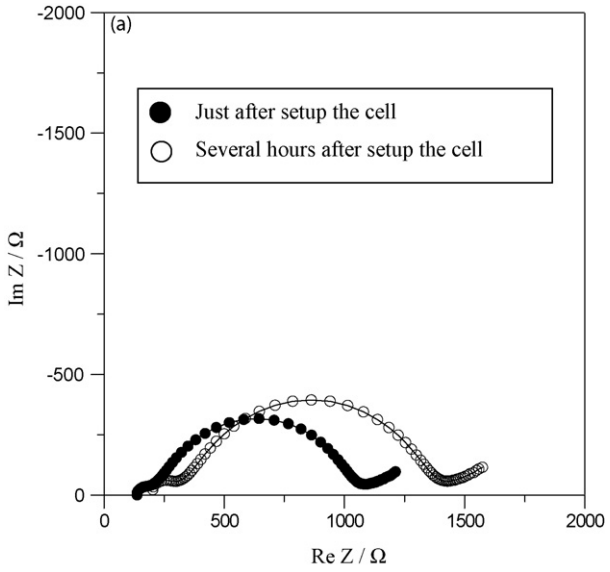

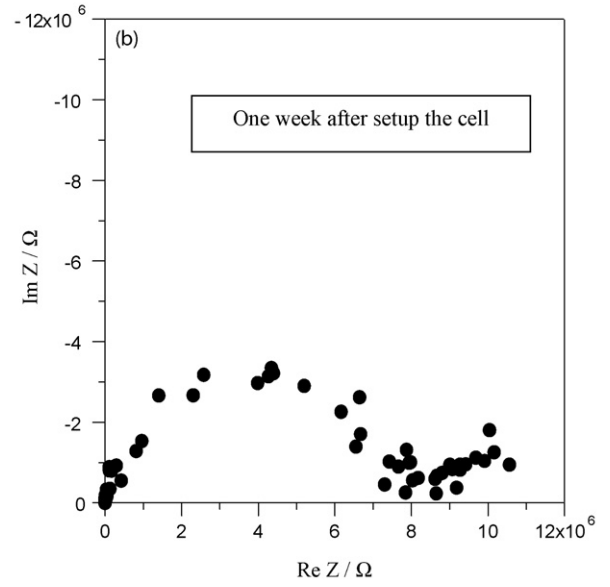

Fig. 5. Time dependence of the impedance spectra of Li–Al/LATP/Li–Al cell at 80 °C.

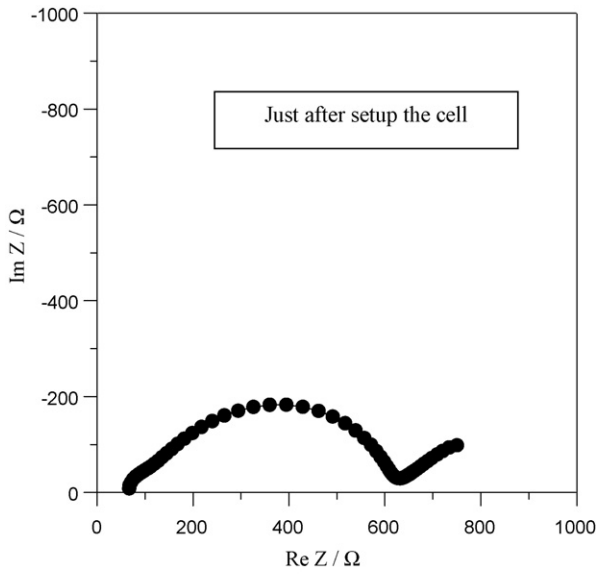

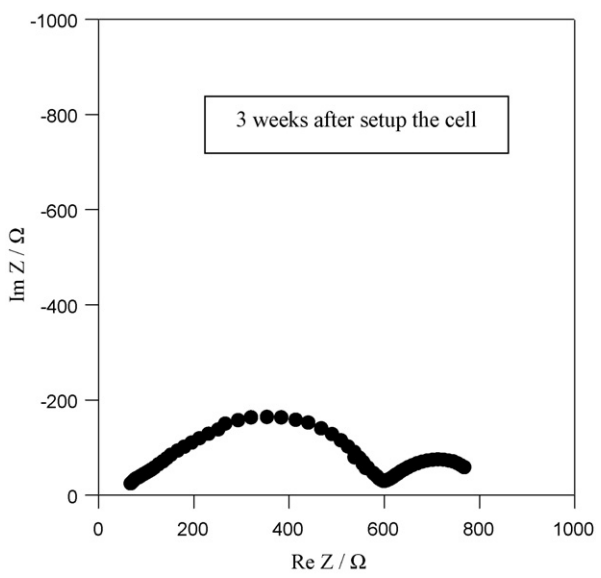

Fig. 6. Time dependence of the impedance spectra of Li–Al/LiPON/LATP/LiPON/Li–Al cell at 80 °C.

about 1×10^{-6} S cm^{-1} and the activation energy for the conduction is 50–60 kJ mol^{-1}. Almost same conductivities were obtained for the LiPON films with different thickness. These conductivity and activation energy for conduction are comparable with those previously reported [13].

LATP is stable in water, but it is not chemically stable in contact with metallic lithium, thus its use in direct contact with a Li anode was precluded. A possible solution to this chemical reactivity issue of the highly conductive and water-stable LATP electrolyte is to form a thin and dense solid electrolyte film directly on the LATP plate. West et al. [14] suggested that a LiPON-coated LATP plate is chemically stable against Li metal. The interface resistances of the Li–Al/LATP/Li–Al and Li–Al/LiPON/LATP/LiPON/Li–Al cells have been examined in a temperature range of 25–80 °C. To make a good contact with a Li sheet, an Al thin film by Rf sputtering was deposited on the LATP plate and the LiPON film, respectively. The cell voltage of the Li–Al/LATP/Li–Al cell showed less than several ten mV to confirm that the Al thin film reacted with Li metal to be a Li–Al alloy.

Fig. 5 shows the ac impedance diagrams (Nyquist plots) of a cell Li–Al/LATP/Li–Al at 80 °C. The cell impedances just after set-up and after several hours show a small semi-circle in a high frequency range and a large semi-circle at a lower frequency range. The second semi-circle was increased with time, which may correspond to the interface impedance between LATP and Li–Al. The interfacial resistance at 80 °C increased to be more than 3 MΩ cm^2 after standing for 1 week at room temperature. It means that LATP reacts with metallic Li to produce insulator phase. The Li–Al/LiPON/LATP/LiPON/Li–Al cell, however, showed a stable interface resistance, where LATP thin film was deposited on the LATP plate to reduce the contact resistance between LiPON and LATP. Fig. 6 shows a typical impedance diagram measured at 80 °C of the Li–Al/LiPON/LATP/LiPON/Li–Al cell just after set-up and after standing for 3 weeks at room temperature. No change in the impedance diagram is observed in the two diagrams, that is, the LiPON layer is quite effective to suppress the reaction of LATP and Li metal. Both impedance diagrams show a slightly distorted large semicircle at a high fre-

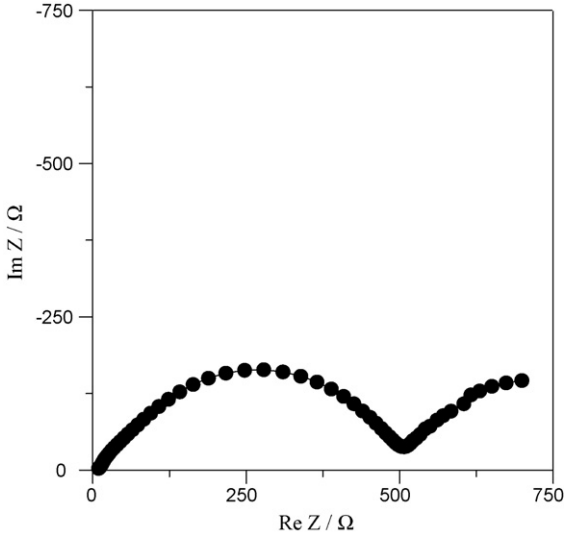

Fig. 7. Impedance spectrum of Li–Al/LiPON/Li–Al cell at 80 °C.

quency range and a part of small semicircle at a low frequency range.

To identify the origins of the resistances, the impedances of the Li–Al/LiPON/Li–Al and Au/LiPON/LATP/LiPON/Au cells have been examined. In Figs. 7 and 8, the impedance diagrams of those cells at 80 °C were shown, respectively. The Au/LiPON/LATP/LiPON/Au cell shows a typical blocking electrode response. The intercept of the semi-circle with the real axis at a higher frequency represents the bulk resistance of LiPON and LATP. Another intercept at a lower frequency shows the total resistance of about 80 Ω including grain boundary in LATP. The Li–Al/LiPON/Li–Al cell shows a distorted semi-circle at high frequencies followed by a semi-circle at low frequencies, which is quite similar to the impedance diagram of the Li–Al/LiPON/LATP/LiPON/Li–Al cell shown in Fig. 6. Hence, these two semi-circles are thought to stem from the LiPON/Li–Al interface. The high frequency part corresponds to the ionic transport resistance between Li–Al and LiPON. It may be due to the solid electrolyte interface (SEI) formed on the lithium electrode and referred as interface resistance hereafter. The low frequency semi-circle

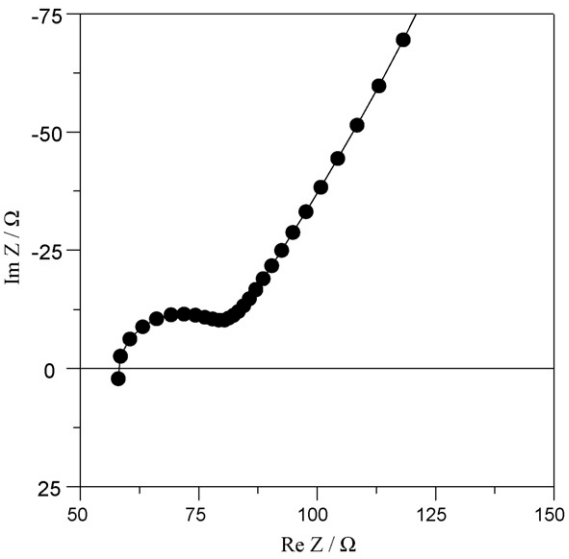

Fig. 8. Impedance spectrum of Au/LiPON/LATP/LiPON/Au cell at 80 °C.

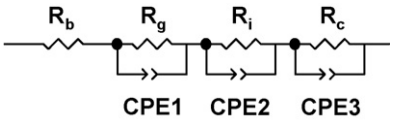

Fig. 9. Equivalent circuit model used to fit the impedance data.

changed by the cell voltage, that is, it corresponds to the charge transfer resistance.

To apply the electrochemical model for the Li–Al/LiPON/LATP/LiPON/Li–Al cell, we considered four resistance components, which are electrolyte bulk (R_b), electrolyte grain boundary (R_g), interface resistance between LiPON and Li–Al (R_i) and charge transfer resistance (R_c). The impedance data of Fig. 6 was fitted to the equivalent circuit model shown in Fig. 9 and compared with the results of Li–Al/LiPON/Li–Al and Au/LiPON/LATP/LiPON/Au. R_b is estimated to be about 21 Ω cm^2 at 80 °C, the value of which is comparable with the bulk resistance of the LiPON film of 23 Ω cm^2. R_g was calculated to be 20 Ω cm^2, which corresponds to the grain boundary resistance of LATP (23 Ω cm^2). The highest resistance is observed in R_i, which is attributed to the interfacial ionic conduction between Li–Al and LiPON. The estimated value of R_i (180 Ω cm^2) is equal to the interface resistance of Li–Al/LiPON (200 Ω cm^2) in Li–Al/LiPON/Li–Al. R_c was estimated to be 120 Ω cm^2, which is comparable to the charge transfer in Li–Al/LiPON/Li–Al.

The temperature dependences of $1/R_g$, $1/R_i$ and $1/R_c$ are shown in Fig. 10. The activation energy of R_g was calculated to be 58 kJ mol^{-1}, which is a slightly higher than that of LATP (50 kJ mol^{-1}). The interface resistance R_i of Li–Al/LiPON shows the activation energy of 60 kJ mol^{-1}, which is comparable with that for

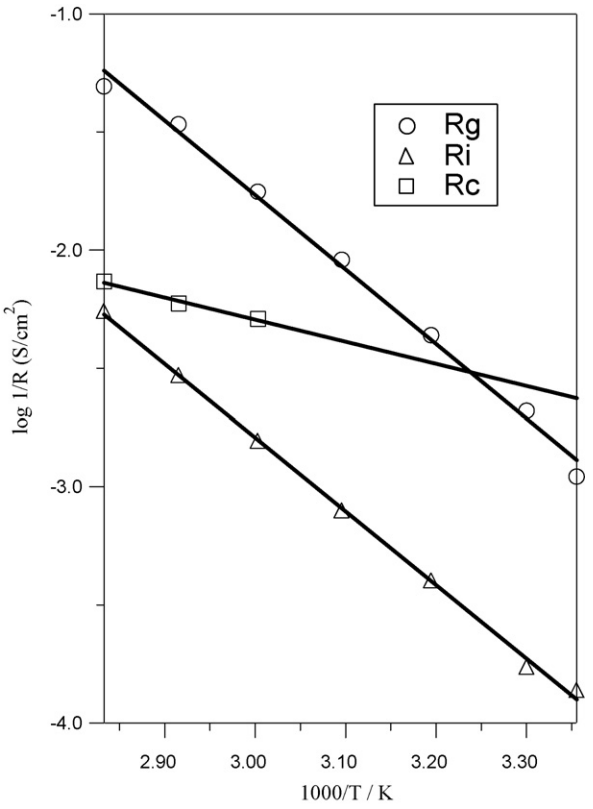

Fig. 10. Temperature dependence of the grain boundary resistance of LATP (R_g), the interface resistance of Li–Al/LiPON (R_i), and the charge transfer resistance (R_c) estimated from the impedance spectra of Li–Al/LiPON/LATP/LiPON/Li–Al cell.

ionic conduction of LiPON. Jeon et al. [15] reported that the large difference of the cell resistances of Li/LiPON/V_2O_5 was observed between the cells prepared in situ and ex situ process. The cell resistance by in situ process was about 400 Ω, but that of ex situ process became 4000 Ω. Iriyama et al. [16] also reported that the cell resistance of Li/LiPON/Li was about 750 Ω cm^2 at room temperature. The high interface resistance may be due to the SEI layer at Li/LiPON by reaction of Li and LiPON under moisture. On the other hand, the activation energy for the charge transfer resistance R_c is as low as 18 kJ mol^{-1}. At higher temperatures, this charge transfer resistance becomes dominant in the total cell resistances.

The conductivity of LiPON seems too low to make ohmic contact with LATP by simple integration of these components. On the impedance measurement in Figs. 6 and 7, LATP thin film was sputtered on both sides of the LATP plate to make ohmic contact with LiPON. The interface resistance at 80 °C of the cell with the sputtered LATP film on the LATP was as high as 216 Ω cm^2, compared to 5.4 kΩ cm^2 for the cell without the sputtered LATP film. The total cell resistance at 25 °C was estimated to be about 8 kΩ cm^2, the value of which is comparable to that of 10 kΩ cm^2 for the Cu-Li/LiPON/LATP/LiPON/Li cell at room temperature [14]. The total cell resistance at 80 °C was 350 Ω cm^2, which is comparable to the dc resistance of 320 Ω cm^2 at the same temperature. These data show that the present composite anode can operate at practical rates at high temperature as 80 °C.

4. Conclusions

The lithium ion conductive solid electrolyte (LATP) supplied by OHARA Inc. showed a high stability against water. The LATP plate immersed in water exhibited no significant conductivity change during 1 month. The sputtered LiPON thin film on the LATP prevented the irreversible reaction of LATP and Li metal from being occurred. However, a high interface resistance between Li–Al and LiPON was observed at lower temperatures. The interface resistance between LiPON and LATP was reduced drastically by sputtering a thin LATP film on the LATP plate. The high interface resistance between LiPON and Li–Al should be reduced for the lower temperature operation of Li-air battery. To achieve this, we should make a good contact between these components and take care of the fabrication atmosphere of the cell.

Acknowledgments

We thank OHARA Inc. for supplying the LATP plate and powder and are grateful Dr Y. Inda of OHARA Inc. for the helpful comments and suggestions.

This research was sponsored by the New Energy and Industrial Technology Development Organization (NEDO) of Japan under the project, Development of High-performance Battery System for Next-generation Vehicles.

References

[1] K.M. Abraham, Z. Jiang, J. Electrochem. Soc. 143 (1996) 1–5.
[2] S.S. Sandhu, J.P. Fellner, G.W. Brutchen, J. Power Sources 164 (2007) 365–371.
[3] J. Read, J. Electrochem. Soc. 149 (2002) A1190–A1195.
[4] T. Kuboki, T. Okuyama, T. Ohsaki, N. Takami, J. Power Sources 146 (2005) 766–769.
[5] A. Debart, M. Holzapfel, P. Novak, T. Ogasawara, P.G. Bruce, IMLB 2006, 2006 (Abstract #521).
[6] S.J. Visco, E. Nimon, B. Katz, L.C.D. Jonghe, M.Y. Chu, IMLB 12, 2004 (Abstract #53).
[7] S.J. Visco, E. Nimon, B. Katz, L.C.D. Jonghe, M.Y. Chu, ECS 210th Meeting, 2006 (Abstract #389).
[8] J. Fu, Solid State Ionics 96 (1997) 195–200.
[9] J. Fu, US Patent No. 5,702,995 (1997).
[10] J.S. Thokchom, B. Kumar, J. Electrochem. Soc. 154 (2007) A331–A336.
[11] J.S. Thokchom, B. Kumar, Solid State Ionics 177 (2006) 727–732.
[12] H. Aono, E. Sugimoto, Y. Sadaoka, N. Imanaka, G. Adachi, J. Electrochem. Soc. 136 (1989) 590–591.
[13] Y. Hamon, A. Douard, F. Sabary, C. Marcel, P. Vinatier, B. Pecquenard, A. Levasseur, Solid State Ionics 177 (2006) 257–261.
[14] W.C. West, J.F. Whitacre, J.R. Lim, J. Power Sources 126 (2004) 134–138.
[15] E.J. Jeon, Y.W. Shin, S.C. Nam, W.I. Cho, Y.S. Yoon, J. Electrochem. Soc. 148 (2001) A318–A322.
[16] Y. Iriyama, T. Kako, C. Yada, T. Abe, Z. Ogumi, Solid State Ionics 176 (2005) 2371–2376.